Three-electron anisotropic quantum dots in variable magnetic fields: exact results for excitation spectra, spin structures, and entanglement

Yuesong Li, Constantine Yannouleas, and Uzi Landman
School of Physics, Georgia Institute of Technology, Atlanta, Georgia 30332-0430
(Dated: 11 October 2007; Physical Review B, **in press**)

Exact-diagonalization calculations for $N = 3$ electrons in anisotropic quantum dots, covering a broad range of confinement anisotropies and strength of inter-electron repulsion, are presented for zero and low magnetic fields. The excitation spectra are analyzed as a function of the strength of the magnetic field and for increasing quantum-dot anisotropy. Analysis of the intrinsic structure of the many-body wave functions through spin-resolved two-point correlations reveals that the electrons tend to localize forming Wigner molecules. For certain ranges of dot parameters (mainly at strong anisotropy), the Wigner molecules acquire a linear geometry, and the associated wave functions with a spin projection $S_z = 1/2$ are similar to the representative class of strongly entangled states referred to as W-states. For other ranges of parameters (mainly at intermediate anisotropy), the Wigner molecules exhibit a more complex structure consisting of two mirror isosceles triangles. This latter structure can be viewed as an embryonic unit of a zig-zag Wigner crystal in quantum wires. The degree of entanglement in three-electron quantum dots can be quantified through the use of the von Neumann entropy.

PACS numbers: 73.21.La, 31.25.-v, 03.67.Mn, 03.65.Ud

I. INTRODUCTION

Three-electron quantum dots are expected to attract a lot of attention in the near future due to several developments, both experimental and theoretical. First, it was recently demonstrated[1–3] that detailed excitation spectra of two-electron quantum dots (in addition to earlier ground-state measurements[4,5]) can be measured, and theoretically understood, as a function of the externally applied magnetic field. Thus, exploration of the excitation spectra of three-electron quantum dots appears to be a next step to be taken. Second, three-qubit electron spin devices are expected to exhibit enhanced efficiency[6–10] for quantum-computing and quantum-information purposes compared to single-qubit and two-qubit ones.

In this paper, we carry out exact diagonalization (EXD) studies for a three-electron single quantum dot under low and moderate magnetic fields. Unlike previous EXD studies[11,12] that focused mainly on the ground states (GSs) of circular quantum dots,[13] we investigate, in addition, the excitation spectra for three electrons in quantum dots with a wide range of anisotropies. Moreover, consideration of anisotropic quantum dots allows us to investigate the structure of the many-body wave functions with respect to strong-correlations effects, such as electron localization and formation of Wigner molecules with a linear or zig-zag geometry.

Most importantly, we investigate here the feasibility of producing model quantum entangled states (i.e., the socalled W states[8,14,15]), which are often employed in the mathematical treatment of quantum information and which have been experimentally realized with ultracold atoms in linear ion traps.[16] We note that a main factor motivating our investigations is the different nature of the entangling agent, namely, the electromagnetic field in the case of heavy ions versus the two-body Coulomb interaction in the case of electrons.

We further mention other recent proposals in the context of solid state electronic devices for producing three-qubit entanglement. In particular, a scheme based on non-interacting electron-hole excitations in the Fermi sea was investigated in Ref. 17. Unlike our present study that focuses on the effect of the interparticle interaction, however, such *interaction-free* entanglement cannot[17] reproduce the symmetric W-state [see Eq. (13) below]. A different proposal[9] for realizing interaction-free entanglement uses pair-correlation functions to study tripartite entanglement shared among the spins of three fermions in a Fermi gas.

The exact diagonalization method that we use for the solution of the Schrödinger equation corresponding to the Hamiltonian of three electrons interacting via a Coulomb potential in an anisotropic quantum dot, in conjunction with an analysis employing spin-resolved two-point correlation functions, allows us to gain deep insights into the nature of electronic states and three-qubit entanglement in real solid state devices. Additionally, the EXD method provides benchmark results, which could be used for assessment of the adequacy and relative accuracy of certain approximation schemes, including the model Heisenberg Hamiltonian for three localized electrons arranged in a ring geometry that was most recently used in an investigation of the entangled ground states in a three-spin-qubit system.[10]

II. OUTLINE OF THE EXACT DIAGONALIZATION MANY-BODY METHOD

We consider three electrons under zero or low magnetic field (B) in a single quantum dot. The corresponding

many-body Hamiltonian is written as

$$\mathcal{H} = \sum_{i=1}^{3} H(i) + \sum_{j>i=1}^{3} \frac{e^2}{\kappa|\mathbf{r}_i - \mathbf{r}_j|}, \quad (1)$$

where κ is the dielectric constant of the semiconductor material (12.5 for GaAs). The single-particle Hamiltonian is given by

$$H = T + V(x,y) + g^*\mu_B B\sigma, \quad (2)$$

where the last term is the Zeeman interaction, with g^* being the effective Landé factor, μ_B the Bohr magneton, B the perpendicular magnetic field, and $\sigma = \pm 1/2$ the spin projection of an individual electron. The kinetic contribution in Eq. (2) is given by

$$T = \frac{[\mathbf{p} - (e/c)\mathbf{A}(\mathbf{r})]^2}{2m^*}, \quad (3)$$

with m^* being the effective mass ($0.067m_e$ for GaAs) and the vector potential $\mathbf{A}(\mathbf{r}) = 0.5(-By\hat{\imath} + Bx\hat{\jmath})$ being taken according to the symmetric gauge. The external confining potential is denoted as $V(x,y)$, where $\mathbf{r} = x\hat{\imath} + y\hat{\jmath}$.

The external potential is modeled by an anisotropic 2D oscillator

$$V(x,y) = \frac{1}{2}m^*(\omega_x^2 x^2 + \omega_y^2 y^2), \quad (4)$$

which reduces to a circular parabolic QD for $\omega_x = \omega_y = \omega_0$. The ratio $\eta = \omega_x/\omega_y$ characterizes the degree of anisotropy of the quantum dot, and it will be referred to thereafter as the anisotropy parameter. Results will be presented for three cases: $\eta = 1$ (circular), $\eta = 0.724$ (slightly anisotropic), and $\eta = 1/2$ (strongly anisotropic).

We find the eigenstates of the many-body Hamiltonian (1) using an exact diagonalization method. Accordingly, we expand the many-body wave function as a linear superposition,

$$\Psi^{\rm EXD}(\mathbf{r}_1,\mathbf{r}_2,\mathbf{r}_3) = \sum_{1\le i<j<k\le 2K} \mathcal{A}_{ijk}|\psi(1;i)\psi(2;j)\psi(3;k)\rangle, \quad (5)$$

where $|\psi(1;i)\psi(2;j)\psi(3;k)\rangle$ denotes a Slater determinant made out of the three spin-orbitals $\psi(1;i)$, $\psi(2;j)$, and $\psi(3;k)$. For the spin orbitals, we use the notation $\psi(1;i) = \varphi_i(1\uparrow)$ if $1 \le i \le K$ and $\psi(1;i) = \varphi_{i-K}(1\downarrow)$ if $K+1 \le i \le 2K$ [and similarly for $\psi(2;j)$ and $\psi(3;k)$]. K is the maximum number of space orbitals $\varphi_i(\mathbf{r})$ that are considered, with $\varphi_i(l\uparrow) \equiv \varphi_i(\mathbf{r}_l)\alpha$ and $\varphi_i(l\downarrow) \equiv \varphi_i(\mathbf{r}_l)\beta$ where α and β denote up and down spins, respectively. The space orbitals $\varphi_i(\mathbf{r})$ are taken to coincide with the real eigenfunctions of a 2D anisotropic oscillator, that is, the index $i \equiv (m,n)$ and $\varphi_i(\mathbf{r}) = X_m(x)Y_n(y)$, with $X_m(Y_n)$ being the eigenfunctions of the corresponding one-dimensional oscillators in the $x(y)$ direction with frequency $\omega_x(\omega_y)$. The parity operator $\mathcal{P}$ yields $\mathcal{P}X_m(x) = (-1)^m X_m(x)$, and similarly for $Y_n(y)$.

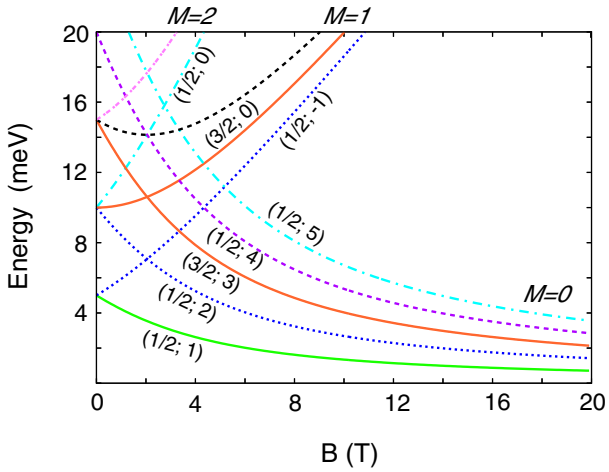

FIG. 1: (Color online) Ground-state and excitation energy spectra [referenced to $3\hbar\sqrt{\omega_0^2 + \omega_c^2/4}$, with $\omega_0 = \sqrt{(\omega_x^2 + \omega_y^2)/2}$] as a function of the magnetic field for $N = 3$ non-interacting electrons in a circular quantum dot ($\eta = 1$). Parameters: external confinement $\hbar\omega_x = \hbar\omega_y = 5$ meV; dielectric constant $\kappa = \infty$; effective mass $m^* = 0.067m_e$, effective Landé coefficient $g^* = 0$. The labels $(S;L)$ denote the quantum numbers for the total spin and the total angular momentum. Different Landau bands are denoted by the different $\mathcal{M}$ values. The S_z indices are not indicated, since the multiplets $(S = 1/2, S_z)$ and $(S = 3/2, S_z)$ are degenerate in energy when $g^* = 0$.

The total energies $E_{\rm EXD}$ and the coefficients $\mathcal{A}_{ijk}$'s are obtained through a direct numerical diagonalization of the matrix eigenvalue equation corresponding to the Hamiltonian in Eq. (1). For the solution of this large scale, but sparse, matrix eigenvalue problem, we have used the ARPACK computer code.[18]

The EXD wave function (5) preserves by construction the third projection S_z of the total spin, since only Slater determinants with a given S_z value are used in the expansion. The exact diagonalization automatically produces eigenfunctions of the square, $\hat{\mathbf{S}}^2$, of the total spin $\hat{\mathbf{S}} = \sum_{i=1}^{3}\hat{\sigma}_i$. The corresponding eigenvalues $S(S+1)$ are calculated with the help of the expression

$$\hat{\mathbf{S}}^2|{\rm SD}\rangle = \left[(N_\alpha - N_\beta)^2/4 + N/2 + \sum_{i<j}\varpi_{ij}\right]|{\rm SD}\rangle, \quad (6)$$

where $|{\rm SD}\rangle$ denotes a Slater determinant and the operator ϖ_{ij} interchanges the spins of electrons i and j provided that their spins are different; N_α and N_β denote the number of spin-up and spin-down electrons, respectively, while N denotes the total number of electrons.

Since the spin orbitals ψ's are orthogonal, the Coulomb matrix elements between two Slater determinants are calculated using the Slater rules,[19] and the necessary two-body matrix elements between space orbitals

$$\int\int d\mathbf{r}_1 d\mathbf{r}_2 \varphi_i^*(\mathbf{r}_1)\varphi_j^*(\mathbf{r}_2)\frac{1}{|\mathbf{r}_1 - \mathbf{r}_2|}\varphi_k(\mathbf{r}_1)\varphi_l(\mathbf{r}_2) \quad (7)$$

are calculated numerically. We have found that this method produces numerically stable results in comparison with algebraic expressions.[20]

III. ENERGY SPECTRA

In this section, we study the ground-state and excitation spectra as a function of an increasing magnetic field B with an emphasis on the role of correlation effects and the influence of the anisotropy.

To better understand the importance of correlations, we first display in Fig. 1 the spectra in the absence of the Coulomb interaction (non-interacting electrons) and for the case of a circular quantum dot. These energy spectra can be determined simply as $\sum_{i=1}^{3}\epsilon_i^{\rm DF}(B)$, where $\epsilon_i^{\rm DF}(B)$ are the Darwin-Fock energies for a single electron.[21–23] The main trend is the formation of three-particle Landau bands (each with an infinite number of states) that tend for $B\to\infty$ to the asymptotic energy levels $(\mathcal{M}+3/2)\hbar\omega_c$, $\mathcal{M}=0,1,2,\ldots$. Note that, for large magnetic fields ($B\to\infty$), the reference energy $3\hbar\sqrt{\omega_0^2+\omega_c^2/4}$, with $\omega_0=\sqrt{(\omega_x^2+\omega_y^2)/2}$, tends to $3\hbar\omega_c/2$. In this limit, the states (S,L), belonging to the same Landau band $\mathcal{M}$, become degenerate in energy, converging to the corresponding familiar Landau level (with index $\mathcal{M}$). Apart from an overall constant, the picture in Fig. 1 is the same as that found in the phenomenological "constant-interaction" model.[23] An important property is the absence of crossings between individual levels within each Landau band. A consequence of this is that the ground state at any B has the same quantum numbers as the one at $B=0$, i.e., it has total spin $S=1/2$ and total angular momentum $L=1$.

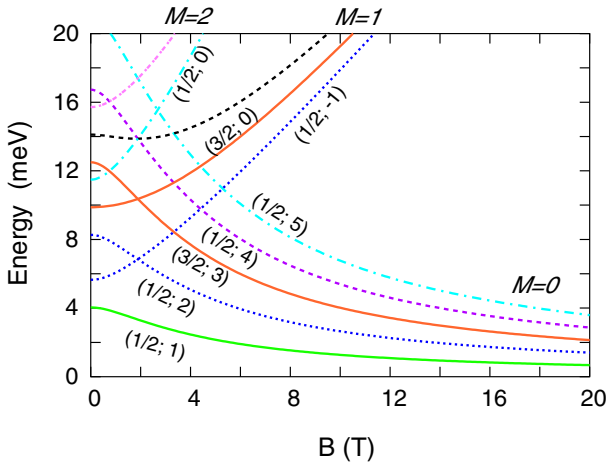

FIG. 2: (Color online) Ground-state and excitation energy spectra [referenced to $3\hbar\sqrt{\omega_0^2+\omega_c^2/4}$, with $\omega_0=\sqrt{(\omega_x^2+\omega_y^2)/2}$ as a function of the magnetic field for $N=3$ non-interacting electrons in a anisotropic quantum dot with anisotropy parameter ($\eta=0.724$). Parameters: external confinement $\hbar\omega_x=4.23$ meV; $\hbar\omega_y=5.84$ meV; dielectric constant $\kappa=\infty$; effective mass $m^*=0.070m_e$, effective Landé coefficient $g^*=0$. The labels $(S;L)$ denote the quantum numbers for the total spin and the total angular momentum in the corresponding circular quantum dot. Although the total angular momentum is not a good quantum number for an anisotropic quantum dot, we retain the labels L here in order to facilitate comparison with the circular case in Fig. 1. The S_z indices are not indicated, since the multiplets $(S=1/2,S_z)$ and $(S=3/2,S_z)$ are degenerate in energy when $g^*=0$.

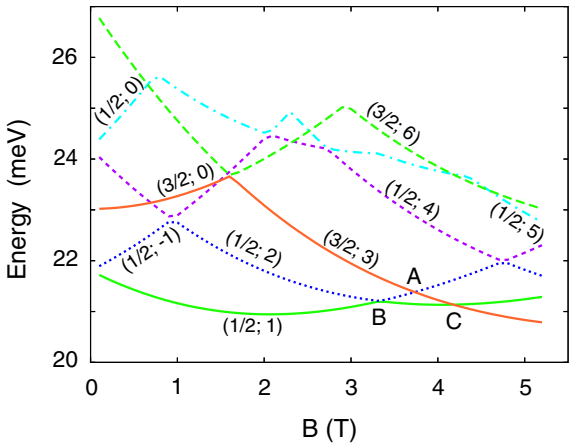

FIG. 3: (Color online) Ground-state and excitation energy spectra [referenced to $3\hbar\sqrt{\omega_0^2+\omega_c^2/4}$, with $\omega_0=\sqrt{(\omega_x^2+\omega_y^2)/2}$ as a function of the magnetic field for $N=3$ interacting electrons in a circular quantum dot ($\eta=1$). Parameters: external confinement $\hbar\omega_x=\hbar\omega_y=5$ meV; dielectric constant $\kappa=12.5$; effective mass $m^*=0.067m_e$; effective Landé coefficient $g^*=0$. The labels $(S;L)$ denote the quantum numbers for the total spin and the total angular momentum. The S_z indices are not indicated, since the multiplets $(S=1/2,S_z)$ and $(S=3/2,S_z)$ are degenerate in energy when $g^*=0$.

The absence of crossings within each Landau band is a characteristic property of non-interacting electrons, and it is independent of the anisotropy of the external confinement. This point is illustrated in Fig. 2 where the non-interacting three-electron spectra are plotted for the case of a quantum-dot with moderate anisotropy ($\eta=0.724$). [for the single-electron energies $\epsilon_i^{\rm DF}(B)$ in an elliptic quantum dot, see Ref. 24 and Ref. 25]. An inspection of Fig. 2 shows that the anisotropy has an effect mainly for small values of the magnetic field (by lifting the degeneracies at $B=0$). On the formation of the Landau bands at higher B, the anisotropy has practically no effect, and, in particular, it cannot induce level crossings within each Landau band).

Another property of the non-interacting spectra is the existence of several degenerate levels (not shown in Figs. 1 and 2) associated with the excited states. We have searched for such degeneracies by inducing a small lifting of them through the artificial use of a very weak Coulomb repulsion specified by $\kappa=200$. For example, in the circular case [see Fig. 1], we found that the state $(1/2;2)$ is doubly degenerate, while the state $(3/2;3)$ is degenerate

with two other $(1/2;3)$ states. These additional states move higher in energy as the strength of the Coulomb interaction increases. We further found that the lifting of degeneracies is sufficiently strong for larger Coulomb repulsions with $\kappa \leq 12.5$ that all the curves in Figs. 3, 4, and 5 below are simple (i.e., the additional states present in the non-interacting case have been pushed much higher and fall outside the energy window shown).

Turning on the interaction introduces correlation effects that lead to important modifications of the non-interacting spectra shown in Figs. 1 and 2. Fig. 3 displays the corresponding spectra for the same circular quantum dot as in Fig. 1, but in the presence of a Coulomb repulsion with $\kappa = 12.5$ (GaAs). Of course, a first effect is the increase in the total energy, but the main difference from the non-interacting case in Fig. 1 is the presence of crossings between levels within the same Landau band. As a result, within the plotted range of magnetic fields, the ground-state total-spin quantum number remains $S = 1/2$ at the first ground-state crossing (at point B), and then it changes to $S = 3/2$ (at the second ground-state crossing at point C). At the same time, the total angular momentum changes from $L = 1$, to $L = 2$, and then to $L = 3$, respectively. As long as the effective Landé coefficient $g^* = 0$, which is the case for the results presented in this section, this threefold alternation in the spin and angular momentum quantum numbers repeats itself ad-infinitum. We note that experimental observation of this threefold alternation may be forthcoming, since quantum dots with a vanishing Landé coefficient have been recently fabricated[1] and were used already to measure two-electron excitation spectra.

The crossings of the curves associated with the three different pairs of quantum numbers $(S = 1/2; L = 1)$, $(1/2;2)$, and $(3/2;3)$ form a small triangle (labeled as ABC), which is located about $B \sim 3.4$ T. Anticipating the results for non-circular dots below, we note that this triangle tends to collapse to a single point with increasing anisotropy.

Another prominent difference between the spectra of non-interacting (Fig. 1) and interacting (Fig. 3) electrons pertains to the degeneracies at $B = 0$ between the $S = 3/2$ and $S = 1/2$ states that are lifted in the interacting-electrons case; compare in particular the curves with quantum numbers $(1/2;2)$ and $(1/2;0)$ with the $(3/2;0)$ one. In contrast, the original degeneracies at $B = 0$ of the $S = 1/2$ states are unaffected by the interelectron interaction; compare the curves $(1/2,1)$ and $(1/2,-1)$, as well as the ones labeled $(1/2,2)$ and $(1/2,0)$. However, these $S = 1/2$ degenaracies at $B = 0$ are lifted as a result of an increasing anisotropy of the quantum dot, as seen in Fig. 4.

Next, we explore the effect of increasing the anisotropy of the quantum dot. In particular, keeping the same strength for the Coulomb interaction ($\kappa = 12.5$), we present two representative anisotropy cases, i.e., $\eta = 0.724$ (intermediate anisotropy, see Fig. 4), and $\eta = 1/2$ (strong anisotropy closer to a quasilinear case, see Fig. 5).

Inspection of the results for the case of intermediate anisotropy (Fig. 4), reveals that compared to Fig. 3 the spectra are distorted, but they maintain the overall topology of the circular dot. As a result, we have been able to use the same pairs of labels in naming the different curves, even though the second label does not have the meaning of an angular momentum (the total angular momentum is not conserved for $\eta \neq 1$). There are two main differences from the circular case: i) the degeneracies at $B = 0$ between the $S = 1/2$ states are lifted, and ii) there is a marked rounding of all the $S = 1/2$ curves in the beginning, so that they do not intersect the vertical energy axis at sharp angles as is the case with Fig. 3. This initial rounding and bending of the energy curves due to the anisotropy has been experimentally observed[1,26] in two-electron quantum dots.

In the case of strong anisotropy (Fig. 5), the spectra have evolved to such an extent that only little relation to the circular case can be traced, and as a result we use a single label signifying the total spin to distinguish them. An important feature that emerges is that the three curves with lowest energies (two $S = 1/2$ and one $S = 3/2$ curve) form a band that is well separated from the other excited states. The existence of such an isolated lowest-energy band is important for validating simple two-qubit and three-qubit models introduced in quantum computation and quantum information theory.[6,27]

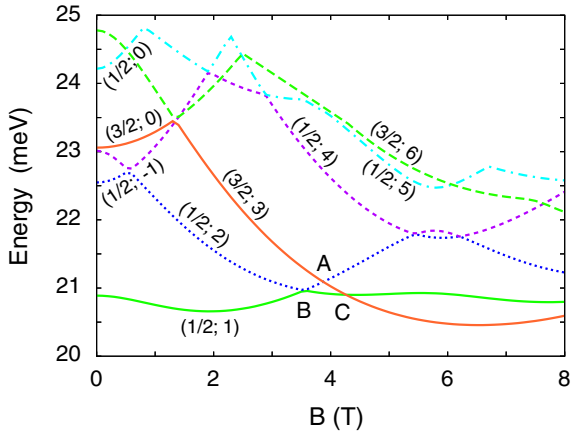

FIG. 4: (Color online) Ground-state and excitation energy spectra [referenced to $3\hbar\sqrt{\omega_0^2+\omega_c^2/4}$, with $\omega_0 = \sqrt{(\omega_x^2+\omega_y^2)/2}$] as a function of the magnetic field for $N = 3$ interacting electrons in an elliptic quantum dot with intermediate anisotropy (anisotropy parameter $\eta = 0.724$). Parameters: external confinement $\hbar\omega_x = 4.23$ meV, $\hbar\omega_y = 5.84$ meV; dielectric constant $\kappa = 12.5$; effective mass $m^* = 0.070m_e$; effective Landé coefficient $g^* = 0$. The labels $(S;L)$ denote the quantum numbers for the total spin and the total angular momentum in the corresponding circular quantum dot. The S_z indices are not indicated, since the multiplets $(S = 1/2, S_z)$ and $(S = 3/2, S_z)$ are degenerate in energy when $g^* = 0$. Note the shrinking of the ABC triangle compared to the $\eta = 1$ case shown in Fig. 3.

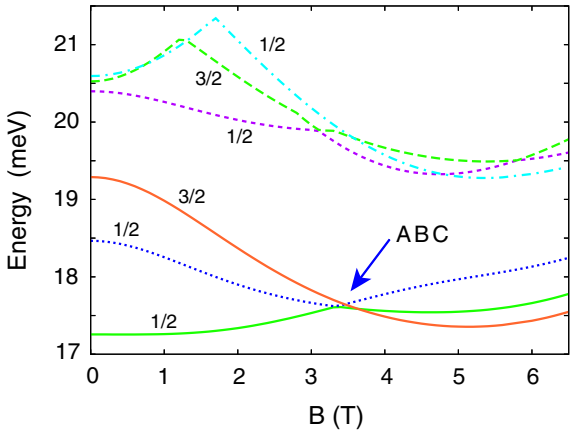

FIG. 5: (Color online) Ground-state and excitation energy spectra [referenced to $3\hbar\sqrt{\omega_0^2+\omega_c^2/4}$, with $\omega_0 = \sqrt{(\omega_x^2+\omega_y^2)/2}$] as a function of the magnetic field for $N = 3$ electrons in an elliptic quantum dot with strong anisotropy (anisotropy parameter $\eta = 1/2$). Parameters: external confinement $\hbar\omega_x = 3.137$ meV, $\hbar\omega_y = 6.274$ meV; dielectric constant $\kappa = 12.5$; effective mass $m^* = 0.067m_e$; effective Landé coefficient $g^* = 0$. The single labels denote the quantum numbers for the total spin. The S_z indices are not indicated, since the multiplets $(S = 1/2, S_z)$ and $(S = 3/2, S_z)$ are degenerate in energy when $g^* = 0$. Note the collapse of the triangle ABC compared to the cases with $\eta = 1$ (Fig. 3) and $\eta = 0.724$ (Fig. 4), and the appearance of a triple-point crossing.

Another remarkable feature of the strong-anisotropy case is the appearance of a non-trivial triple-point crossing lying on the ground-state curve (see arrow in Fig. 5), which is created from the collapse of the ABC triangle between the two $S = 1/2$ and the one $S = 3/2$ lowest-in-energy curves (compare Figs. 3 and 4). This low-energy non-trivial triple point [forming within the lowest Landau band ($\mathcal{M} = 0$)] is due to the effect of the Coulomb interaction, and it is to be contrasted to other trivial triple-point crossings at much higher energies arising from the intersection of the lowest Landau band with the $\mathcal{M} = 1$ and $\mathcal{M} = 2$ higher Landau bands, and which are present even in the non-interacting limit [see, e.g., the triple crossing at (2.0 T; 14.2 meV) in Fig. 1]. It would be of interest to analyze whether the recently observed[28] triple-point crossings in deformed quantum dots are non-trivial or trivial in the sense described above.

Before leaving this Section, we note that the spin multiplets $(S = 1/2, S_z)$ and $(S = 3/2, S_z)$ are degenerate in energy when $g^* = 0$, which was the case for the energy spectra presented in Figs. 1-5. At a given magnetic field, this degeneracy is naturally lifted when $g^* \neq 0$; however, the final total energies can be easily calculated by adding the Zeeman term $g^*\mu_B B S_z$ to the spectral curves displayed in these figures. Furthermore, for a given pair (S, S_z), the Zeeman term does not influence the intrinsic structure of the many-body EXD wave function [i.e., the expansion over constituent Slater determinants, see Eq. (5)], and thus taking $g^* = 0$ does not effect the results for

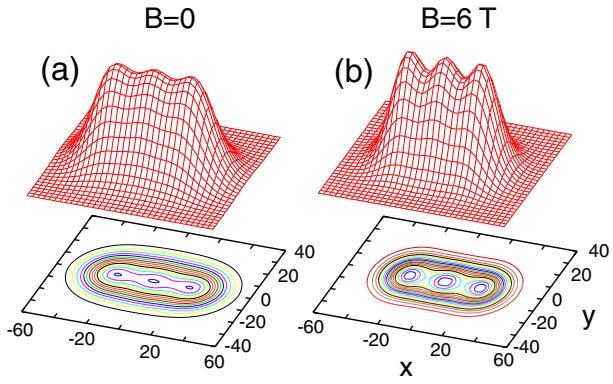

FIG. 6: (Color online) Exact-diagonalization electron densities for the ground states of $N = 3$ electrons in an anisotropic dot with parameters $\hbar\omega_x = 3.137$ meV, $\hbar\omega_y = 6.274$ meV ($\eta = 1/2$), effective mass $m^* = 0.067m_e$, dielectric constant $\kappa = 12.5$ (GaAs). (a): The case of zero magnetic field, $B = 0$. (b) The case with a magnetic field $B = 6$ T. Lengths in nm. The electron densities are in arbitrary units, but with the same scale in both panels.

electron densities, conditional probability distributions, and von Neumann entropies presented below.

IV. MANY-BODY WAVE FUNCTIONS FOR STRONG ANISOTROPY ($\eta = 1/2$)

A. $S = 1/2$ ground states: Evolution of electron densities as a function of the inter-electron repulsion

When the confining potential lacks circular symmetry, charge localization is reflected directly in the single-particle electron densities. Indeed, electron localization is visible in Figs. 6 and 7, which display the electron densities for $N = 3$ electrons in an anisotropic quantum dot with $\eta = 1/2$. Fig. 6 illustrates the evolution of electron localization with increasing magnetic field in the case of a weaker Coulomb repulsion ($\kappa = 12.5$). One sees that already at $B = 0$, the electron density is shaped linearly for all practical purposes. However, the three peaks of the localized electrons are rather weak, which contrasts with the case of $B = 6$ T [Fig. 6(b)], where the three electron peaks are sharply defined.

Fig. 7 [in conjunction with Fig. 6(a)] illustrates the strengthening of electron localization as a function of increasing Coulomb repulsion, i.e., decreasing dielectric constant κ, from a value of 12.5 [Fig. 6(a)] to $\kappa = 3$ [Fig. 7(a)] and then to $\kappa = 1$ [Fig. 7(b)]. In this last case [Fig. 7(b)], the three electrons are almost fully localized, with orbitals that exhibit practically zero mutual overlap.

Since we keep the average frequency, $\omega_0 = \sqrt{(\omega_x^2+\omega_x^2)/2}$, approximately constant (i.e., $\hbar\omega_0 \approx 5.0$ meV) for all anisotropy cases studied in this paper, decreasing the dielectric constant is equivalent to increasing the Wigner parameter[29] R_W. At zero magnetic field,

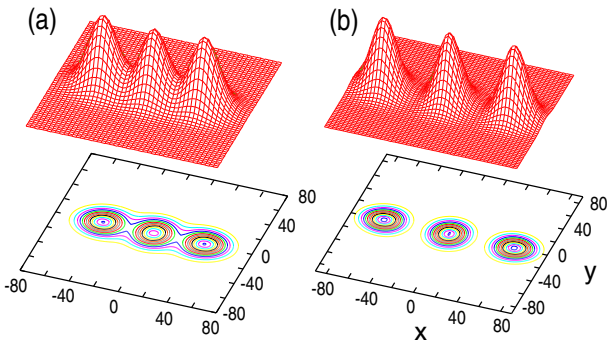

FIG. 7: (Color online) Exact-diagonalization electron densities at zero magnetic field ($B = 0$) for the ground state of $N = 3$ electrons in an anisotropic dot with parameters $\hbar\omega_x = 3.137$ meV, $\hbar\omega_y = 6.274$ meV ($\eta = 1/2$), $m^* = 0.067m_e$. (a): dielectric constant $\kappa = 3.0$. (b): dielectric constant $\kappa = 1.0$. Lengths in nm. The electron densities are in arbitrary units, but with the same scale as in Fig. 6 for both panels.

R_W is widely used as a universal parameter to indicate the strength of correlations, since it provides the relative strength of the Coulomb repulsion with respect to the quantum kinetic energy, i.e.,

$$R_W = \frac{e^2/(\kappa l_0)}{\hbar\omega_0}, \tag{8}$$

with the characteristic length $l_0 = \sqrt{\hbar/(m^*\omega_0)}$. For the numerical values of R_W associated with the cases studied here, see Fig. 15.

B. $S = 1/2$ ground state: Spin resolved intrinsic structure for strong repulsion ($\kappa = 1$)

In the previous section, we saw that already the electron densities provide partial information about the formation of a linear Wigner molecule within an elliptic quantum dot. Indeed, from the charge distributions in Figs. 6 and 7, one can infer that the electrons are localized in three separate positions $\mathbf{R}_1$, $\mathbf{R}_2$, and $\mathbf{R}_3$. If the electrons were spinless, this situation could be approximately reproduced by a single Slater determinant denoted as $|\bigcirc\bigcirc\bigcirc\rangle$. However, to probe the spin distribution of the electrons, the exact-diagonalization charge densities do not suffice; one needs to consider spin-resolved two-point correlation functions, defined as

$$P_{\sigma\sigma_0}(\mathbf{r},\mathbf{r}_0) = \langle\Psi^{\rm EXD}|\sum_{i\neq j}\delta(\mathbf{r}-\mathbf{r}_i)\delta(\mathbf{r}_0-\mathbf{r}_j)\delta_{\sigma\sigma_i}\delta_{\sigma_0\sigma_j}|\Psi^{\rm EXD}\rangle, \tag{9}$$

with the EXD many-body wave function given by equation (5).

Using a normalization constant

$$\mathcal{N}(\sigma,\sigma_0,\mathbf{r}_0) = \int P_{\sigma\sigma_0}(\mathbf{r},\mathbf{r}_0)d\mathbf{r}, \tag{10}$$

we further define a related conditional probability distribution (CPD) as

$$\mathcal{P}_{\sigma\sigma_0}(\mathbf{r},\mathbf{r}_0) = P_{\sigma\sigma_0}(\mathbf{r},\mathbf{r}_0)/\mathcal{N}(\sigma,\sigma_0,\mathbf{r}_0), \tag{11}$$

having the property $\int \mathcal{P}_{\sigma\sigma_0}(\mathbf{r},\mathbf{r}_0)d\mathbf{r} = 1$. The spin-resolved CPD gives the spatial probability distribution of finding the remaining electrons with spin projection σ under the condition that the third electron is located (fixed) at $\mathbf{r}_0$ with spin projection σ_0; σ and σ_0 can be either up ($\uparrow$) or down ($\downarrow$).

Before examining such CPDs, evaluated for numerically determined EXD wave functions, it is instructive to consider on a qualitative level the spin structure of the wave functions that can be formed from three localized spin-orbitals only. In particular, we focus on the case with a total spin projection $S_z = 1/2$, when the most general three-orbital wave function is given by the superposition of three Slater determinants, i.e., by the expression

$$\Phi(S_z = \tfrac{1}{2}) = a|\uparrow\downarrow\uparrow\rangle + b|\uparrow\uparrow\downarrow\rangle + c|\downarrow\uparrow\uparrow\rangle, \tag{12}$$

with the normalization $a^2+b^2+c^2 = 1$. Unlike the circles used earlier to indicate spinless electrons, the arrows in Eq. (12) indicate the spin projections of the individual spin-orbitals.

The general states (12) are a superposition of three Slater determinants and have attracted a lot of attention in the mathematical theory of entanglement. Indeed, they represent a prototypical class of three-qubit entangled states known as W-states.[15] For general coefficients a, b, and c, the states (12) are not eigenfunctions of the square of total spin $\hat{\mathbf{S}}^2$ (while the exact-diagonalization wave functions in Eq. (5 are always good eigenfunctions of $\hat{\mathbf{S}}^2$). However, the special values of these coefficients that lead to good total-spin quantum numbers can be determined.[7,30] In particular, using the notation $\Phi(S, S_z; i)$ (where the index i is employed in case of a degeneracy), one has

$$\sqrt{3}\Phi(\tfrac{3}{2},\tfrac{1}{2}) = |\uparrow\downarrow\uparrow\rangle + |\uparrow\uparrow\downarrow\rangle + |\downarrow\uparrow\uparrow\rangle \tag{13}$$

(i.e., $a = b = c = 1/\sqrt{3}$),

$$\sqrt{6}\Phi(\tfrac{1}{2},\tfrac{1}{2};1) = 2|\uparrow\downarrow\uparrow\rangle - |\uparrow\uparrow\downarrow\rangle - |\downarrow\uparrow\uparrow\rangle \tag{14}$$

(i.e., $a = 2/\sqrt{6}$, $b = c = -1/\sqrt{6}$),

$$\sqrt{2}\Phi(\tfrac{1}{2},\tfrac{1}{2};2) = |\uparrow\uparrow\downarrow\rangle - |\downarrow\uparrow\uparrow\rangle \tag{15}$$

(i.e., $a = 0$, $b = 1/\sqrt{2}$, $c = -1/\sqrt{2}$).

For completeness, we list the case for three fully spin-polarized localized electrons (which of course is not a W-state).

$$\Phi(\tfrac{3}{2},\tfrac{3}{2}) = |\uparrow\uparrow\uparrow\rangle. \tag{16}$$

The wave functions with projections $S_z = -1/2$ and $S_z = -3/2$ are similar to the above, but with inverted single-particle spins.

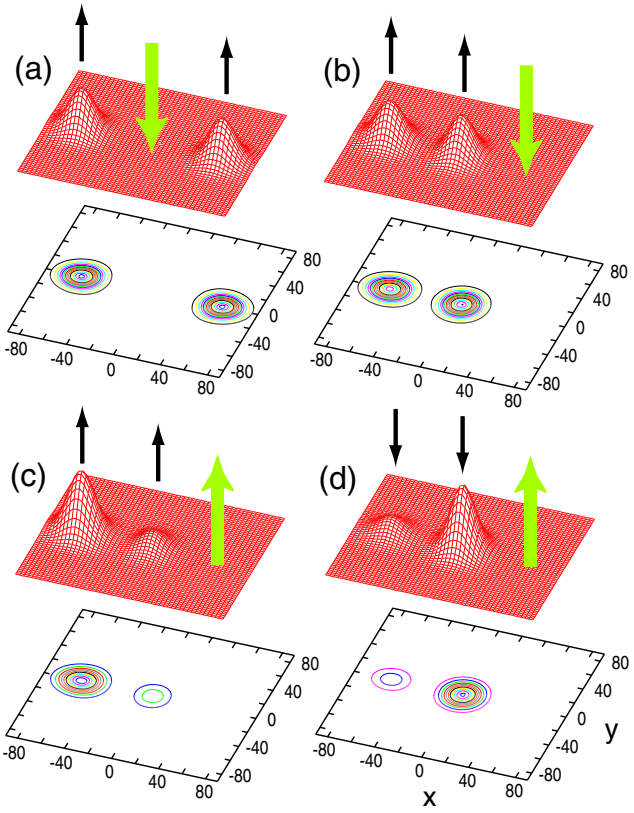

FIG. 8: (Color online) Spin-resolved conditional probability distributions for the (1/2,1/2) ground state of $N = 3$ electrons in an anisotropic dot at zero magnetic field ($B = 0$) with parameters $\hbar\omega_x = 3.137$ meV, $\hbar\omega_y = 6.274$ meV ($\eta = 1/2$), $m^* = 0.067m_e$ and $\kappa = 1$ [for the corresponding electron density, see Fig. 7(b)]. The heavy arrow (green online) indicates the location of the fixed electron at $\mathbf{r}_0$ [see Eq. (11)], with the indicated spin projection σ_0, i.e., up ($\uparrow$) or down ($\downarrow$). (a) $\uparrow\downarrow$ CPD with the fixed spin-down electron located at the center. (b) $\uparrow\downarrow$ CPD with the fixed spin-down electron located on the right. (c) $\uparrow\uparrow$ CPD with the fixed spin-up electron located on the right. (d) $\downarrow\uparrow$ CPD with the fixed spin-up electron located on the right. The spin of the fixed electron is denoted by a thick arrow (green online). Lengths in nanometers. The vertical axes are in arbitrary units, but the scale is the same for all four panels.

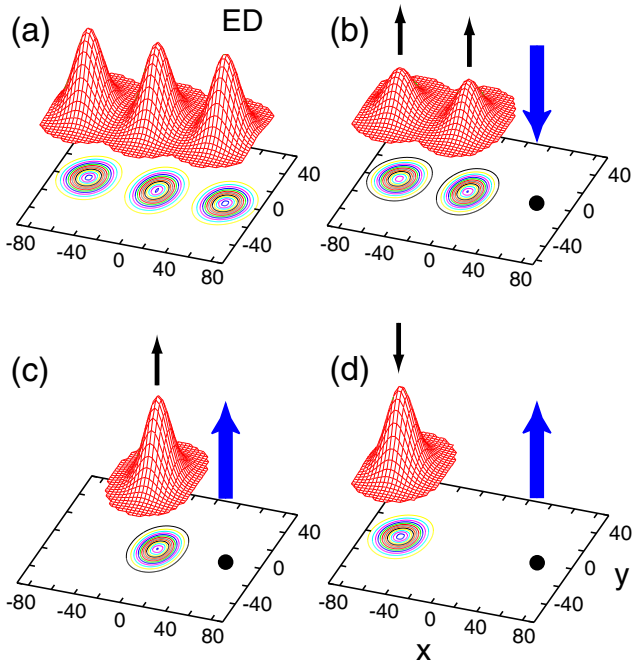

FIG. 9: (Color online) Spin-resolved conditional probability distributions for the (1/2,1/2) first excited state of $N = 3$ electrons in an anisotropic dot at zero magnetic field ($B = 0$) with parameters $\hbar\omega_x = 3.137$ meV, $\hbar\omega_y = 6.274$ meV ($\eta = 1/2$), $m^* = 0.067m_e$ and $\kappa = 1$. (a) electron density (ED). (b) $\uparrow\downarrow$ CPD with the fixed spin-down electron located on the right at (61,0). (c) $\uparrow\uparrow$ CPD with the fixed spin-up electron located on the right at (61,0). (d) $\downarrow\uparrow$ CPD with the fixed spin-up electron located at the right at (61,0). The spin of the fixed electron is denoted by a thick arrow (blue online). Lengths in nanometers. The vertical axes are in arbitrary units, but the scale is the same for all four panels.

Before proceeding further, we note that the term W-state is some times reserved for the symmetric form $\Phi(\frac{3}{2},\frac{1}{2})$ in Eq. (13). This symmetric W-state has been experimentally realized in linear ion traps.[16] As we show below, quantum dots offer the means for generating in addition the less symmetric forms given by Eqs. (14) and (15). Such nonsymmetric three-qubit states are sometime denoted[31] as W'-states (with a prime). In this paper, we do not make use of this distinction, and we refer to both symmetric and nonsymmetric forms simply as W-states.

In Fig. 8, we present several spin-resolved CPDs associated with the EXD ground state at $B = 0$ and strong anisotropy $\eta = 1/2$, which is a $\Psi^{\rm EXD}(1/2, 1/2)$ state [see Fig. 5]. Although the EXD expansion in Eq. (5) consists of a large number of Slater determinants built from delocalized harmonic-oscillator orbitals, the CPD patterns in Fig. 8 reveal an intrinsic structure similar to that of the wave function $\Phi(\frac{1}{2},\frac{1}{2};1)$ in Eq. (14), which is made out of only three localized spin-orbitals. In particular, when one requires that the fixed electron has a down spin and is located at the center of the quantum dot, the spin-up electrons are located on the left and right with equal weights [Fig. 8(a)]. Keeping the down spin-direction, but moving the fixed electron to the right, reveals that the spin-up electrons are located on the left and the center with equal weights [Fig. 8(b)]. Considering a spin-up direction for the fixed electron and placing it on the right reveals that the remaining spin-up electron is distributed on the left and the center of the quantum dot with unequal weights; approximately 4 (left) to 1 (center) following the square of the coefficients in front of the determinants $|\uparrow\downarrow\uparrow\rangle$ ($a = 2/\sqrt{6}$) and $|\downarrow\uparrow\uparrow\rangle$ ($c = 1/\sqrt{6}$) in the wave function $\Phi(\frac{1}{2},\frac{1}{2};1)$ [see Eq. (14)]. Similarly, considering a spin-up direction for the fixed electron and placing it on the right reveals that the spin-down electron is distributed

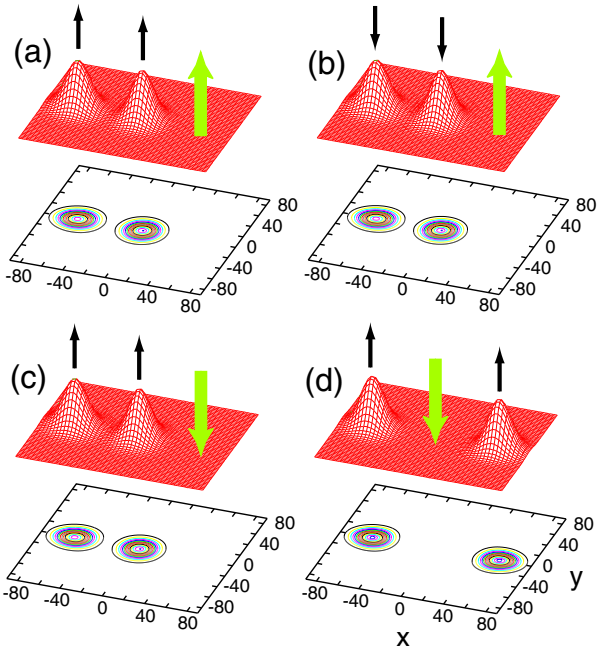

FIG. 10: (Color online) Spin-resolved conditional probability distributions for the (3/2,1/2) second excited state of $N = 3$ electrons in an anisotropic dot at zero magnetic field ($B = 0$) with parameters $\hbar\omega_x = 3.137$ meV, $\hbar\omega_y = 6.274$ meV ($\eta = 1/2$), $m^* = 0.067m_e$ and $\kappa = 1$. (a) $\uparrow\uparrow$ CPD with the fixed spin-up electron located on the right at (70,0). (b) $\downarrow\uparrow$ CPD with the fixed spin-up electron located on the right at (70,0). (c) $\uparrow\downarrow$ CPD with the fixed spin-down electron located on the right at (70,0). (d) $\uparrow\downarrow$ CPD with the fixed spin-down electron located at the center. The spin of the fixed electron is denoted by a thick arrow (green online). Lengths in nanometers. The vertical axes are in arbitrary units, but the scale is the same for all four panels.

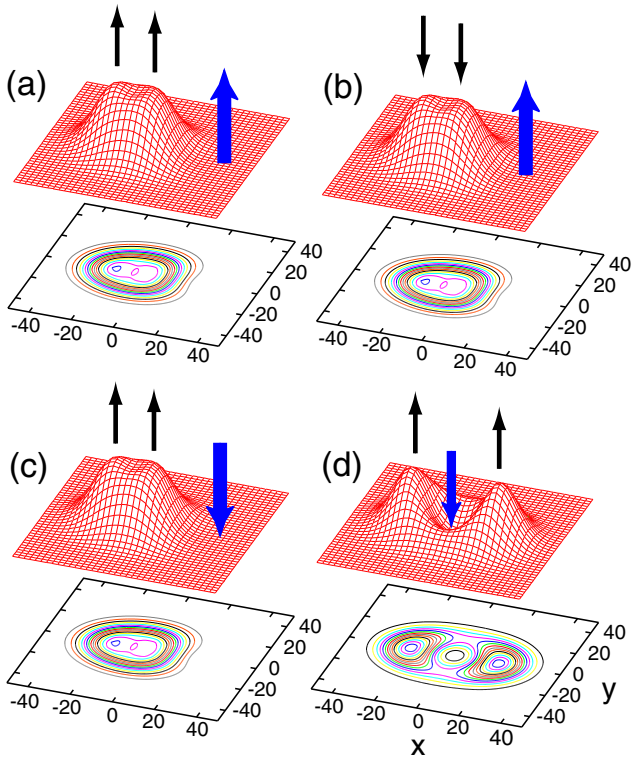

FIG. 11: (Color online) Spin-resolved conditional probability distributions for the (3/2,1/2) ground state of $N = 3$ electrons in an anisotropic dot at $B = 5$ T with parameters $\hbar\omega_x = 4.23$ meV, $\hbar\omega_y = 5.84$ meV ($\eta = 0.724$), $m^* = 0.070m_e$ and $\kappa = 12.5$. (a) $\uparrow\uparrow$ CPD with the fixed spin-up electron located on the right at (30,0). (b) $\downarrow\uparrow$ CPD with the fixed spin-up electron located on the right at (30,0). (c) $\uparrow\downarrow$ CPD with the fixed spin-down electron located on the right at (30,0). (d) $\uparrow\downarrow$ CPD with the fixed spin-down electron located at the center. The spin of the fixed electron is denoted by a thick arrow (blue online). Lengths in nanometers. The vertical axes are in arbitrary units, but the scale is the same for all four panels.

on the left and the center of the quantum dot with unequal weights – approximately 1 (left) to 4 (center), in agreement with the weights of the Slater determinants in Eq. (14).

C. $S = 1/2$ first excited state: Spin resolved intrinsic structure for strong repulsion ($\kappa = 1$)

In section IV B, we investigated the intrinsic structure of the ground-state three-electron wave functions with total spin $S = 1/2$ and for the case of a strong anisotropy $\eta = 1/2$. In this section, we analyze a case of the first-excited EXD wave function with total spin $S = 1/2$ and for the same strong anisotropy $\eta = 1/2$, again at $B = 0$ T and for strong interelectron repulsion $\kappa = 1$. We denote this state as $\Psi^{\rm EXD}(1/2, 1/2; 2)$.

In Fig. 9(a), we display the electron density (ED) for this second $S = 1/2$ state, while in Figs. 9(b,c,d), we display spin-resolved CPDs for the same state. From the charge density, we conclude that the three electrons form a sharply defined linear Wigner molecule. The spin-resolved CPD with a spin-down fixed electron placed on the right [see Fig. 9(b)] is similar to that in Fig. 8(b). However, the two spin-resolved CPDs with a *spin-up* fixed electron placed on the right [see Figs. 9(c) and 9(d)] are quite different from the corresponding CPDs in Figs. 8(c) and 8(d). In fact, in both cases, only one single hump appears to the left of the fixed electron, located at the center for the remaining spin-up electrons [Fig. 9(c)], or on the left for the remaining spin-down electrons [Fig. 9(d)].

This indicates that the intrinsic structure of the $\Psi^{\rm EXD}(1/2, 1/2; 2)$ wave function is close to that of $\Phi(\frac{1}{2}, \frac{1}{2}; 2)$ in Eq. (15), with $a = 0$ and $b = -c$.

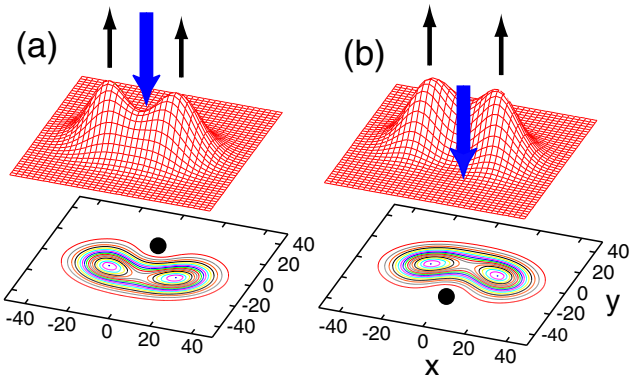

FIG. 12: (Color online) Spin-resolved conditional probability distributions for the (3/2,1/2) ground state of $N = 3$ electrons in an anisotropic dot at $B = 5$ T with parameters $\hbar\omega_x = 4.23$ meV, $\hbar\omega_y = 5.84$ meV ($\eta = 0.724$), $m^* = 0.070m_e$ and $\kappa = 12.5$. (a) $\uparrow\downarrow$ CPD with the fixed spin-down electron located on the y-axis at (0,20) (solid dot). (b) $\uparrow\downarrow$ CPD with the fixed spin-down electron located on the y-axis at (0,-20) (solid dot). The spin of the fixed electron is denoted by a thick arrow (blue online). Lengths in nanometers. The vertical axes are in arbitrary units, but the scale is the same for all panels in this figure and in Fig. 11.

D. $S = 3/2$ second excited state: Spin resolved intrinsic structure for strong repulsion ($\kappa = 1$)

In sections IV B and IV C, we investigated the intrinsic structure of the many-body three-electron wave functions with total spin $S = 1/2$ and for the case of a strong anisotropy $\eta = 1/2$. In this section, we analyze a case of an EXD wave function with total spin $S = 3/2$ and for the same strong anisotropy $\eta = 1/2$, again at $B = 0$ T. In particular, we analyze the intrinsic structure of a $\Psi^{\rm EXD}(3/2, 1/2)$ wave function that is the second excited state for these parameters.

In Fig. 10, we display spin-resolved CPDs for this $S = 3/2$ excited state. A remarkable feature is that for a fixed electron placed on the right all three CPDS, $\uparrow\uparrow$ [Fig. 10(a)], $\downarrow\uparrow$ [Fig. 10(b)], and $\uparrow\downarrow$ [Fig. 10(c)] coincide. This indicates that the intrinsic structure of the $\Psi^{\rm EXD}(3/2, 1/2)$ wave function is close to that of $\Phi(\frac{3}{2}, \frac{1}{2})$ in Eq. (13), with all three coefficients equal to each other, i.e., $a = b = c$.

Taking into account the $\uparrow\downarrow$ CPD with the fixed electron at the center of the quantum dot, it is clear that the geometric arrangement of the three localized electrons is linear. Arrangements that are more complicated than the linear geometry can emerge, however, for a range of different parameters, as is discussed in section V A below.

V. MANY-BODY WAVE FUNCTIONS FOR INTERMEDIATE ANISOTROPY ($\eta = 0.724$)

A. Moderate repulsion ($\kappa = 12.5$)

In this section, we analyze a case of an EXD wave function with total spin $S = 3/2$ and for the intermediate anisotropy $\eta = 0.724$. In particular, we analyze the intrinsic structure of a $\Psi^{\rm EXD}(3/2, 1/2)$ wave function that is the ground state at a magnetic field $B = 5$ T (see Fig. 4).

In Fig. 11, we display spin-resolved CPDs for this ground state. A remarkable feature is that for a fixed electron placed on the right all three CPDS, $\uparrow\uparrow$ [Fig. 11(a)], $\downarrow\uparrow$ [Fig. 11(b)], and $\uparrow\downarrow$ [Fig. 11(c)] coincide. This indicates that the intrinsic structure of the $\Psi^{\rm EXD}(3/2, 1/2)$ wave function is close to that of $\Phi(\frac{3}{2}, \frac{1}{2})$ in Eq. (13), with all three coefficients equal to each other, $a = b = c$.

However, these CPDs, as well as the $\uparrow\downarrow$ CPD with the fixed spin-down electron at the center [Fig. 11(d)], are broader along the y-direction compared to the CPDs associated with the linear molecular arrangement in Fig. 10. This suggests that, for an intermediate anisotropy ($\eta = 0.724$), the intrinsic structure of $\Psi^{\rm EXD}(3/2, 1/2)$ is more complicated. Indeed, as demonstrated in Fig. 12 where the fixed spin-down electron is successively placed away from the x-axis at (0, 20 nm) and at (0, -20 nm), the intrinsic structure corresponds to a superposition of two molecular isomers, each one described by a three-orbital wave function $\Phi(\frac{3}{2}, \frac{1}{2})$, but with the three localized spin-orbitals located on the vertices of two isosceles triangles, each one being a mirror reflection (relative to the x-axis) of the other. The base of the first isosceles triangle lies at -6 nm [Fig. 12(a)] and that of the second one at 6 nm [Fig. 12(a)] off the x-axis (in the y-direction).

The two-triangle configuration discussed for three electrons above may be seen as the embryonic precursor of a quasilinear structure of two intertwined "zig-zag" crystalline chains. Such *double* zig-zag crystalline chains may also be related to the *single* zig-zag Wigner-crystal chains discussed recently in relation to spontaneous spin polarization in quantum wires.[32,33]

It is interesting to inquire of how this two-triangle structure is reflected in the spatial distribution of the electron densities. Indeed, in Fig. 13(a), we display the electron density associated with the (3/2,1/2) ground state at $B = 5$ T. We note in particular the absence of a third peak at the center of the quantum dot. Instead, two rather small peaks appear at (0,20 nm) and (0,-20 nm), in agreement with the two-triangle internal structure revealed by the CPD analysis.

B. Strong repulsion ($\kappa = 1$)

We further display in Fig. 13(b) the corresponding electron density for the (1/2,1/2) ground state at $B = 0$

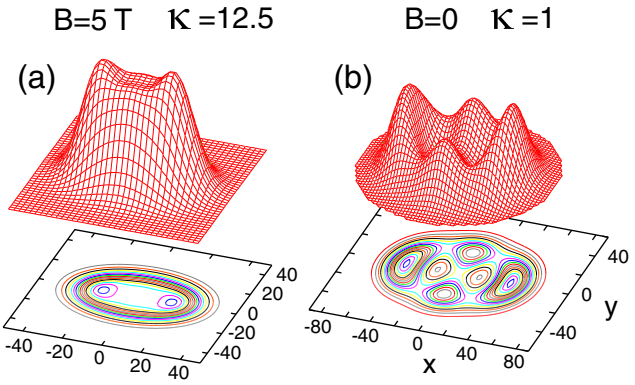

FIG. 13: (Color online) Exact-diagonalization electron densities for the ground state of $N = 3$ electrons in an anisotropic quantum dot with parameters $\hbar\omega_x = 4.23$ meV, $\hbar\omega_y = 5.84$ meV ($\eta = 0.724$, intermediate anisotropy) and $m^* = 0.070m_e$. (a) the (3/2,1/2) ground state at $B = 5$ T and $\kappa = 12.5$. (b) the (1/2,1/2) ground state at $B = 0$ and $\kappa = 1$ (strong interelectron repulsion). Lengths in nm. The electron densities are in arbitrary units, with a different scale in each panel.

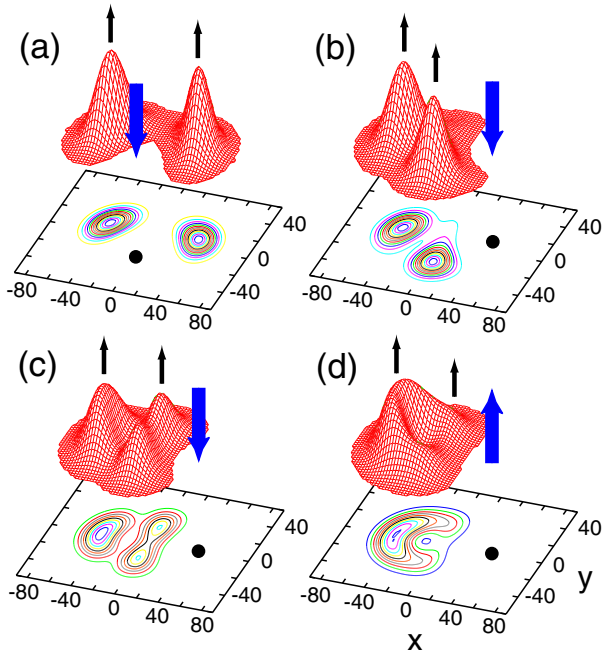

FIG. 14: (Color online) Spin-resolved conditional probability distributions for the (1/2,1/2) ground state of $N = 3$ electrons in an anisotropic dot at $B = 0$ with parameters $\hbar\omega_x = 4.23$ meV, $\hbar\omega_y = 5.84$ meV ($\eta = 0.724$), $m^* = 0.070m_e$ and $\kappa = 1$. (a) $\uparrow\downarrow$ CPD with the fixed spin-down electron located on the y-axis at (0,-20) (solid dot). (b) $\uparrow\downarrow$ CPD with the fixed spin-down electron located off center at (40,11) (solid dot). (c) $\uparrow\downarrow$ CPD with the fixed spin-down electron located on the x-axis at (43,0) (solid dot). (d) $\uparrow\uparrow$ CPD with the fixed spin-ip electron located on the x-axis at (43,0) (solid dot). The spin of the fixed electron is denoted by a thick arrow (blue online). Lengths in nanometers. The vertical axes are in arbitrary units, but the scale is the same for all panels in this figure.

and for a strong Coulomb repulsion ($\kappa = 1$) at the intermediate anisotropy $\eta = 0.724$. As a result of the enhanced electron localization, the electron density exhibits pronounced peaks whose locations form a clearly defined diamond; this indicates again the presence of a two-triangle internal configuration.[34] The detailed interlocking of the two triangular configurations is further revealed in the spin-resolved CPDs that are displayed in Fig. 14. From the CPDs in Figs. 14(a) and 14(b), it can be concluded that one triangle is formed by the points $\mathbf{R}_1 \approx (0, -20)$ nm, $\mathbf{R}_2 \approx (-43, 10)$ nm, and $\mathbf{R}_3 \approx (43, 10)$ nm, while the second one (its mirror) is formed by the points $\mathbf{R}'_1 \approx (0, 20)$ nm, $\mathbf{R}'_2 \approx (-43, -10)$ nm, and $\mathbf{R}'_3 \approx (43, -10)$ nm. The $\uparrow\downarrow$ [Fig. 14(c)] and $\uparrow\uparrow$ [Fig. 14(d)] CPDS with the fixed electron on the right at (43,0) nm are similar to those in Figs. 8(b) and 8(c), respectively, with the difference that the central hump is clearly a double one. This indicates that each triangular configuration is associated with a wave function of the form $\Phi(\frac{1}{2}, \frac{1}{2}; 1)$ given in Eq. (14).

Naturally, the regime of a linear configuration versus a two-triangle one depends on both the strength of the interaction and the anisotropy. Detailed studies of the phase boundary between these two intrinsic structures are, however, left for a future investigation.

VI. DEGREE OF ENTANGLEMENT

The many-body wave functions for $N = 3$ electrons analyzed in the previous sections are highly entangled states, since they cannot be reduced to a single Slater determinant. For special ranges of the dot parameters, we showed that they acquire the same internal structure as the prototypical W-states. In this section, we demonstrate that the degree of entanglement can be further quantified through the use of the von Neumann entropy $\mathcal{S}_{\rm vN}$ for indistinguishable fermions which (in analogy to the two-electron case[35–38]) is defined as

$$\mathcal{S}_{\rm vN} = -{\rm Tr}(\rho \log_2 \rho) + \mathcal{C}, \tag{17}$$

where $\mathcal{C}$ is a constant (see below for choosing its value) and the single-particle density matrix is given by

$$\rho_{\nu\mu} = \frac{\langle \Psi^{\rm EXD} | a^\dagger_\mu a_\nu | \Psi^{\rm EXD} \rangle}{\sum_\mu \langle \Psi^{\rm EXD} | a^\dagger_\mu a_\mu | \Psi^{\rm EXD} \rangle}, \tag{18}$$

and is normalized to unity, i.e., ${\rm Tr}\rho = 1$. The Greek indices μ (or ν) count the spin orbitals $\psi(\mathbf{r}; \mu)$ that span the single-particle space (of dimension $2K$; see Section II). Note that, in keeping with previous literature on two electrons,[35,37,38] the logarithms are taken to base two.

Naturally, for calculating numerically the matrix ele-

ments $\rho_{\nu\mu}$, we use the expansion (5) to get

$$\langle \Psi^{\rm EXD}|a^\dagger_\mu a_\nu|\Psi^{\rm EXD}\rangle = \sum_{I,J} \mathcal{A}^*_I \mathcal{A}_J \langle {\rm SD}(I)|a^\dagger_\mu a_\nu|{\rm SD}(J)\rangle, \tag{19}$$

where the following conventions for the indices I (or J) apply: $I \to (ijk)$ and $|{\rm SD}(I)\rangle = |\psi(1;i)\psi(2;j)\psi(3;k)\rangle$. The matrix elements $\langle {\rm SD}(I)|a^\dagger_\mu a_\nu|{\rm SD}(J)\rangle$ between Slater determinants that enter in Eq. (19) simply equal ± 1 or vanish. The single-particle density ρ in Eq. (18) is in general non-diagonal. Thus we further perform numerically a diagonalization of ρ, and we use the new diagonal elements $\tilde{\rho}_{\mu\mu}$ to straightforwardly calculate the von Neumann entropy in Eq. (17).

As was discussed in Refs. 36–38, the von Neumann entropy provides a natural measure of entanglement in the case of interacting indistinguishable fermions. In this case, the entanglement is related[39] to quantum correlations that are intrinsic to the many-body wave function, i.e., $\mathcal{S}_{\rm vN}$ quantifies the fact that strongly correlated states comprise a larger number of significant Slater determinants compared to weakly correlated ones. Accordingly, one expects that $\mathcal{S}_{\rm vN}$ increases when the many-body correlations increase (i.e., when R_W and B increase). This was the case indeed for the $N = 2$ quantum dot,[37,38] but we have found that it also holds true for the $N = 3$ quantum dot, as can be seen from Fig. 15 and Fig. 16.

In the case when the many-body wave function reduces to a single Slater determinant, i.e., when the expansion coefficients reduce to $\mathcal{A}_I = \delta_{I,I_0}$, all the matrix elements $\rho_{\mu\nu}$ vanish except three diagonal ones (corresponding to three fully occupied spin orbitals) which are equal to $1/3$; then $-{\rm Tr}(\rho \log_2 \rho) = \log_2 3 = 1.5850$. Since the entanglement due to the Pauli exchange principle by itself cannot be used as a resource for quantum-information processing,[36,40] we take the constant $\mathcal{C}$ in Eq. (17) to be

$$\mathcal{C} = -\log_2 N, \tag{20}$$

and as a result the von Neumann entropy for a single Slater determinant vanishes in our convention.

In Fig. 15, we plot the von Neumann entropy for the three lowest EXD states with $S_z = 1/2$ as a function of κ (R_W) for $N = 3$ electrons in an anisotropic quantum dot for a strong anisotropy with anisotropy parameter $\eta = 1/2$. It is apparent that the von Neumann entropy increases for all three states as R_W increases (κ decreases) and the electrons become more localized.

At $\kappa = 12.50$ (corresponding to weaker correlations), the von Neumann entropies for the three states are clearly non-vanishing, indicating that these EXD states are far from being close to a single Slater determinant. On the other hand, it is natural to expect that the EXD states will reduce to single Slater determinants at the non-interacting limit. To check this expectation, we have carried out an EXD calculation for the same QD parameters described in the caption of Fig. 15, but with a very large $\kappa = 10000$ in order to approximately mimick the non-interacting limit. In this latter case, we found

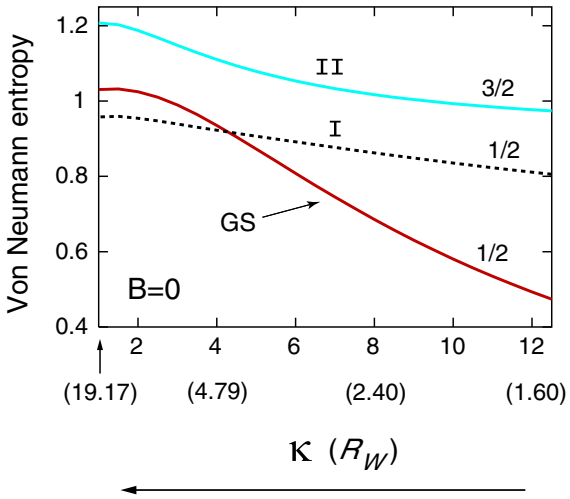

FIG. 15: (Color online) Von Neumann entropy at zero magnetic field for the three lowest EXD states with $S_z = 1/2$ as a function of the dielectric constant κ [or equivalently the Wigner parameter R_W; see Eq. (8)] for $N = 3$ electrons in an anisotropic quantum dot with strong anisotropy (anisotropy parameter $\eta = 1/2$). Parameters: external confinement $\hbar\omega_x = 3.137$ meV, $\hbar\omega_y = 6.274$ meV; effective mass $m^* = 0.067 m_e$. The single labels 3/2 and 1/2 denote the quantum numbers for the total spin. The ground state (GS), and the first (I) and second (II) excited states are indicated. The horizontal arrow indicates the direction of increasing correlations. According to our convention, the von Neumann entropy for a single determinant vanishes. Although the energy gaps between the three EXD states diminish with decreasing κ (they are quasidegenerate for $\kappa = 1$), the relative energy ordering remains unchanged in the plotted range.

that indeed the ground state [with $(S = 1/2; S_z = 1/2)$ is practically a single Slater determinant made out from the three spin orbitals $(m = 0, n = 0; \uparrow)$, $(m = 0, n = 0; \downarrow)$, and $(m = 1, n = 0; \uparrow)$ [the lowest-in-energy spatial orbital $(m = 0, n = 0)$ being doubly occupied; see Section II for the meaning of indices m and n). We also found that the corresponding $S_{\rm vN}$ is practically zero.

However, due to the $\eta = 1/2$ anisotropy, one has $2\hbar\omega_x = \hbar\omega_y$, which gives rise to a high degree of energy degeneracy among excited Slater determinants with good total spin. For example, the Slater determinant $|(m = 0, n = 0; \uparrow), (m = 1, n = 0; \downarrow), (m = 1, n = 0; \uparrow)\rangle$ is degenerate to the determinant $|(m = 0, n = 0; \uparrow), (m = 0, n = 0; \downarrow), (m = 0, n = 1; \uparrow)\rangle$. In this situation, a small $e - e$ interaction is sufficient to produce strong mixing of the degenerate Slater determinants, and as a result the corresponding $S_{\rm vN}$ values for excited states were found to be non-vanishing. These findings are reflected in Fig. 15 where, for $\kappa = 12.50$ (weakest Coulomb repulsion in the plotted range), the $S_{\rm vN}$ value for the EXD ground state is noticeably lower than the values for the two excited states.

As was demonstrated in Section IV, at zero magnetic field and strong Coulomb repulsion (e.g., $\kappa = 1$), the three electrons are well separated and localized, and their

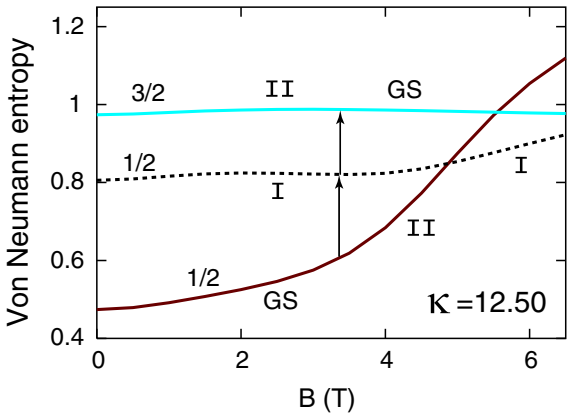

FIG. 16: (Color online) Von Neumann entropy for the three lowest EXD states with $S_z = 1/2$ as a function of the magnetic field for $N = 3$ electrons in an anisotropic quantum dot with strong anisotropy (anisotropy parameter $\eta = 1/2$). Parameters: external confinement $\hbar\omega_x = 3.137$ meV, $\hbar\omega_y = 6.274$ meV; dielectric constant $\kappa = 12.5$; effective mass $m^* = 0.067m_e$. The single labels 3/2 and 1/2 denote the quantum numbers for the total spin. The vertical arrows indicate the discontinuous jump in the von Neumann entropy of the ground state at $B = 3.4$ T, where the ground-state quantum numbers change character, first from $(1/2, 1/2; 1)$ to $(1/2, 1/2; 2)$, and then immediately to $(3/2, 1/2)$. The ground state (GS), and the first (I) and second (II) excited states are indicated, both to the left and to the right of the vertical arrows. According to our convention, the von Neumann entropy for a single determinant vanishes.

EXD wave functions are equivalent to the forms given in Eq. (14) (GS), Eq. (15) (first excited state, I), and Eq. (13) (second excited state, II). These forms are special cases of the general form in Eq. (12) for which another measure of entanglement, called the tangle and specifying the reduced tripartite entanglement among the three localized spin qubits,[15] can be applied.

The tangle can be calculated[15] from the coefficients a, b, and c, and it was found that it vanishes for all cases covered by the general form in Eq. (12). In this respect, the von Neumann entropy for three well separated electrons studied here exhibits qualitatively a very different behavior, since the values of $S_{\rm vN}$ at $\kappa = 1$ are all different, as seen from Fig. 15. In particular, we note that in this case the EXD value of $S_{\rm vN}$ for the I state is lower than that of the GS state; this naturally reflects the fact that the first excited EXD state in this limit is effectively composed of only two Slater determinants [see Eq. (15)] compared to the three Slater determinants associated [see Eq. (14)] with the EXD ground state.

In Fig. 16, we plot the von Neumann entropy for the three lowest EXD states with $S_z = 1/2$ as a function of the magnetic field for $N = 3$ electrons in an anisotropic quantum dot with the same parameters as those for the energy spectra in Fig. 5 (strong anisotropy with anisotropy parameter $\eta = 1/2$, as also was the case with Fig. 15). It is apparent that the von Neumann entropy increases for all three states as the magnetic field increases and the electrons become more localized. An interesting feature is the discontinuous jump (around $B = 3.4$ T) in the von Neumann entropy of the EXD ground state. This jump is illustrated by the vertical arrows and is associated with the triple ABC point in Fig. 5. This discontinuity in the ground-state $S_{\rm vN}$ arises from the sudden change in the intrinsic structure (in term of constituent Slater determinants) of the ground state, as the latter changes its quantum numbers first from $(1/2, 1/2; 1)$ to $(1/2, 1/2; 2)$, and then again immediately to $(3/2, 1/2)$ at the triple point.

VII. SUMMARY

We have presented extensive exact-diagonalization calculations for $N = 3$ electrons in anisotropic quantum dots, and for a broad range of anisotropies and strength of inter-electron repulsion. We have analyzed the excitation spectra both as a function of the magnetic field and as a function of increasing anisotropy. A main finding was the appearance of triple-crossing points in the ground-state energy curves for stronger anisotropies.

Analysis of the intrinsic structure of the many-body wave functions through spin-resolved conditional probability distributions revealed that for all examined cases (including those with parameters corresponding to currently fabricated quantum dots) the electrons localize forming Wigner molecules. For certain ranges of dot parameters (mainly at strong anisotropy), the Wigner molecules acquire a linear geometry, and the associated wave functions with a spin projection $S_z = 1/2$ are similar to the socalled W-states that are a prototype of entangled states. For other ranges of parameters (mainly at intermediate anisotropy), the Wigner molecules exhibit a more complex structure consisting of two mirror isosceles triangles. This latter structures can be considered as an embryonic unit of a zig-zag Wigner crystal in quantum wires.

Finally, we demonstrated that the degree of entanglement in three-electron quantum dots can be quantified via the von Neumann entropy, in analogy with studies on two-electron quantum dots.

[1] C. Ellenberger, T. Ihn, C. Yannouleas, U. Landman, K. Ensslin, D. Driscoll, and A.C. Gossard, Phys. Rev. Lett. **96**, 126806 (2006).

[2] D.M. Zümbuhl, C.M. Marcus, M.P. Hanson, and A.C. Gossard, Phys. Rev. Lett. **93**, 256801 (2004).

[3] Y. Nishi, P.A. Maksym, D.G. Austing, T. Hatano, L.P.

Kouwenhoven, H. Aoki, and S. Tarucha, Phys. Rev. B **74**, 033306 (2006).
[4] S. Tarucha, D.G. Austing, T. Honda, R.J. van der Hage, and L.P. Kouwenhoven, Phys. Rev. Lett. **77**, 3613 (1996).
[5] M. Ciorga, A.S. Sachrajda, P. Hawrylak, C. Gould, P. Zawadzki, S. Jullian, Y. Feng, and Z. Wasilewski, Phys. Rev. B **61** R16315 (2000).
[6] F. Meier, J. Levy, and D. Loss, Phys. Rev. Lett. **90**, 047901 (2003).
[7] R. Woodworth, A. Mizel, and D.A. Lidar, J. Phys.: Condens. Matter **18**, S721 (2006).
[8] V.N. Gorbachev and A.I. Trubilko, Laser Phys. Lett. **3**, 59 (2006).
[9] T. Vértesi, Phys. Rev. A **75**, 042330 (2007).
[10] B. Röthlisberger, J. Lehmann, D.S. Saraga, Ph. Traber, and D. Loss, arXiv:0705.1710v1 (2007).
[11] P. Hawrylak, Phys. Rev. Lett. **71** 3347 (1993).
[12] S.A. Mikhailov and N.A. Savostianova, Phys. Rev. B **66**, 033307 (2002).
[13] Szafran *et al.* [B. Szafran, F.M. Peeters, S. Bednarek, and J. Adamowski, Phys. Rev. B **69**, 125344 (2004)] have studied the ground states of three fully spin-polarized electrons in anisotropic quantum dots at high magnetic fields. They used a configuration-interaction scheme with a multicenter basis of floating Gaussians centered around different sites. Unlike the present work, spin-dependent cases at low magnetic fields were not considered by Szafran *et al.*
[14] W. Dür, G. Vidal, and J.I. Cirac, Phys. Rev. A **62**, 062314 (2000).
[15] V. Coffman, J. Kundu, and W.K. Wootters, Phys. Rev. A **61**, 052306 (2000).
[16] C.F. Roos, M. Riebe, H. Häffner, W. Hänsel, J. Benhelm, G.P.T. Lancaster, C. Becher, F. Schmidt-Kaler, and R. Blatt, Science **304**, 1478 (2004).
[17] C.W.J. Beenakker, C. Emary, and M. Kindermann, Phys. Rev. B **69**, 115320 (2004).
[18] R.B. Lehoucq, D.C. Sorensen, and C. Yang, *ARPACK Users' Guide: Solution of Large-Scale Eigenvalue Problems with Implicitly Restarted Arnoldi Methods* (SIAM, Philadelphia, 1998).
[19] A. Szabo and N.S. Ostlund, *Modern Quantum Chemistry* (McGraw-Hill, New York, 1989).
[20] When the orbitals $\varphi_i(\mathbf{r})$ are eigenfunctions of a 2D oscillator, analytic expressions for the Coulomb matrix elements in Eq. (7) have been reported by, e.g., S.M. Girvin and T. Jach [Phys. Rev. B **28**, 4506 (1983)] for a circular oscillator, and Ref. 25 for an anisotropic one.
[21] C.G. Darwin, Proc. Cambridge Philos. Soc. **27**, 86 (1930).
[22] V. Fock, Z. Phys. **47**, 446 (1928).
[23] L.P. Kouwenhoven, D.G. Austing, and S. Tarucha, Rep. Prog. Phys. **64**, 701 (2001).
[24] A.V. Madhav and T. Chakraborty, Phys. Rev. B **49**, 8163 (1994).
[25] J. Kyriakidis and S.J. Penney, Phys. Rev. B **71**, 125332 (2005).
[26] J. Kyriakidis, M. Pioro-Ladriere, M. Ciorga, A.S. Sachrajda, and P. Hawrylak, Phys. Rev. B **66**, 035320 (2002).
[27] J. Kyriakidis and G. Burkard, Phys. Rev. B **75**, 115324 (2007).
[28] D.G. Austing, G. Yu, C. Payette, J.A. Gupta, M. Korkusinski, and G.C. Aers, phys. stat. sol. (a) **204**, 508 (2007).
[29] C. Yannouleas and U. Landman, Phys. Rev. Lett. **82**, 5325 (1999); (Erratum) **85**, 2220 (2000)
[30] R. Pauncz, *The Construction of Spin Eigenfunctions: An Exercise Book* (Kluwer Academic/Plenum Publishers, New York, 2000).
[31] Z.-L. Cao and M. Yang, J. Phys. B **36**, 4245 (2003).
[32] A.D. Klironomos, J.S. Meyer, and K.A. Matveev, Europhys. Lett. **74**, 679 (2006).
[33] G. Piacente, I.V. Schweigert, J.J. Betouras, and F.M. Peeters, Phys. Rev. B **69**, 045324 (2004).
[34] For the two-triangle configuration at high B and for the case of the $(3/2, 3/2)$ fully spin-polarized state, see also Ref. 13.
[35] R. Paskauskas and L. You, Phys. Rev. A **64**, 042310 (2001).
[36] F. Buscemi, P. Bordone, and A. Bertoni, Phys. Rev. A **73**, 052312 (2006).
[37] For EXD calculations of the von Neumann entropy in a two-electron anisotropic quantum dot, see T. Ihn, C. Ellenberger, K. Ensslin, C. Yannouleas, U. Landman, D.C. Driscoll, A.C. Gossard, Int. J. Mod. Phys. B **21**, 1316 (2007).
[38] C. Yannouleas and U. Landman, Rep. Prog. Phys. (2007), in press.
[39] K. Eckert, J. Schliemann, D. Bruss, and M. Lewenstein, Ann. of Phys. (New York) **299**, 88 (2002).
[40] G.C. Ghirardi and L. Marinatto, Phys. Rev. A **70**, 012109 (2004).